Journal of Structural Engineering & Applied Mechanics (2022) 5(4):238-248
DOI 10.31462/jseam.2022.04238248

RESEARCH ARTICLE

Numerical investigation on DE-strengthened-RC beams without steel shear reinforcement

Kağan Söğüt*

Kilis 7 Aralık University, Department of Civil Engineering, Kilis, Türkiye

Article History

Received 24 October 2022
Accepted 23 December 2022

Keywords

Beam
Concrete
Embedded steel bars
Finite element
Shear strengthening

Abstract

This study presents a two-dimensional nonlinear finite element (FE) model for Deep Embedment (DE) strengthened reinforced concrete (RC) beams without existing steel shear links. The FE model was developed and validated against experimental results reported in published literature. The parametric study was thereafter conducted to examine important parameters influencing the strengthened behavior. The parameters were concrete compressive strength, beam width, beam size, and tension reinforcement ratio. The FE model accurately predicted experimental results with a mean predicted-to-experimental value of 1.04. The FE results showed that the percentage of shear strength provided by embedded steel bars was almost constant once both concrete strength and tension reinforcement ratio were increased. However, an increase in the beam width resulted in a decrease in the percentage of shear strength gain due to embedded steel bars. Shear stress at failure decreased once beam size was increased for both unstrengthened (control) and DE-strengthened beams. The percentage of shear strength provided by embedded steel bars decreased from 47.9% to 27.6% as effective depth was increased from 261.5 mm to 523 mm.

1. Introduction

Shear-deficient reinforced concrete (RC) beams have to be strengthened in cases where they exhibit substandard conditions [1-4]. Strengthening solutions have therefore gained importance to provide these beams with adequate shear strength capacity [5]. It has been recognized that the Deep embedment (DE), also called the embedded through section (ETS), is one of the most effective techniques to strengthen existing RC beams in shear [3-8]. In this technique [5-8], the vertical or inclined holes are produced along the shear span by using a drill. This is followed by a procedure consisting of filling holes with epoxy. Steel or fibre-reinforced polymer (FRP) bars are thereafter inserted into holes filled with epoxy. Previous research studies on this technique proved that this technique has been superior to externally bonded (EB) and near-surface mounted (NSM) techniques in cases where strengthening material is not properly anchored to the concrete [4, 7, 9]. It has also been demonstrated that this technique is the most practical solution when it is impossible to access the bottom and/or side faces of the beam [3, 6].

Previous experimental and numerical research studies investigated the important parameters impacting the DE-strengthened behavior [e.g., 3-12]. For example, the impacts of embedded FRP and steel reinforcement

* Corresponding author (kagan.sogut@kilis.edu.tr)

eISSN 2630-5763

ratio [4-6, 8, 11, 13], existing shear reinforcement ratio [3, 5, 8, 14, 15], the inclination angle of embedded FRP or steel bar [8, 14, 15], anchored embedded FRP bar [15], prestressed embedded steel bars [16], and corroded shear links were investigated [17]. However, the DE technique is a relatively new shear strengthening technique, and it is, therefore, vital to examine the impacts of concrete strength, beam size, beam width, and tension reinforcement ratio, which has received little or no attention [12, 18, 19]. The impacts of these parameters on the behavior of DE-strengthened RC beams without steel shear links may play an important role in determining the effectiveness of this technique. The effect of beam width on the behavior of DE-strengthened RC beams without steel shear links was only investigated by Barros and Dalfre [15] in which RC beams were used to validate a finite element (FE) model in this study. The impact of the tension reinforcement ratio on the behavior of DE-strengthened beams without steel shear links has not yet been reported. The effect of beam size in DE-strengthened RC rectangular beams without steel shear links has also not been investigated up to date. This paper reports the effects of concrete strength, beam size, beam width, and tension reinforcement ratio on the DE-strengthened RC rectangular beams without existing steel shear links using FE modeling. The developed FE model, which gives accurate predictions, is presented in this paper. Moreover, a parametric study was conducted using the developed FE model.

2. Summary of experimental study

Two series of RC beams tested by Barros and Dalfre [15] were used to validate the FE model. Each series consisted of an unstrengthened (control) RC beam and a strengthened RC beam with embedded steel bars. As presented in Figure 1, the RC rectangular beams had a width of either 150 mm or 300 mm, an overall depth of 300 mm, and an effective depth of 261.5 mm. All beams had a shear span-to-effective depth (a/d) ratio of 3.44 and were tested in a three-point bending configuration. The first series of tested beams, namely A1 and A3, were longitudinally reinforced in tension and compression with two 25- and 12-mm diameter steel bars, respectively. The compression and tension reinforcement of the second series beams (B1 and B3) comprised three 12- and 25-mm diameter steel bars, respectively. The non-tested spans of RC beams were reinforced in shear with 6 mm diameter steel shear links spaced at 75 mm, whereas the tested spans of RC beams were designed without any shear reinforcement (see Fig. 1). The DE shear strengthening scheme of A3 and B3, respectively, consisted of one 10 mm diameter steel bar and two 8 mm diameter steel bars spaced as shown Fig. 1. The average cylinder concrete compressive strength was 30.78 MPa for both series of tested beams. The mechanical properties of steel bars are reported in Table 1.

3. Finite element modeling

VecTor2 software package which utilities the theoretical background of the Disturbed Stress Field Model (DSFM) [20], which includes improved formulations and assumptions of Modified Compression Field Theory (MCFT) [21] was used to develop a two-dimensional FE model [22]. Fig. 2 demonstrates a developed typical FE model to predict the structural behavior of the beams tested by Barros and Dalfre [15]. A brief explanation of the geometrical details and material models used in this study is given in the following subsections.

3.1. Geometric modeling

A two-dimensional four-node rectangular plane stress element with a total of eight degrees of freedom was used to model concrete, loading, and support steel plates. Bažant and Oh [23] recommended that the average mesh size could be taken as three times the maximum aggregate size. Dirar et al. [24] and Sogut et al. [25] also successfully simulated both unstrengthened and FRP-strengthened RC beams by taking into account an

average mesh size of 2.5 times the maximum aggregate size. Based on the recommendations and good agreement between FE and test results, the average mesh size of 25 mm was taken in each direction.

A two-node truss element with a total of four degrees of freedom was used to model steel reinforcement consisting of tension and compression reinforcement, shear links, and embedded bars. The shear failure was observed during physical tests [15], and the failure mechanism was not affected by the bond behavior. It was therefore assumed that a perfect bond existed between the concrete and steel reinforcement. Sogut et al. [4], Qapo et al. [12], Godat et al. [26], Dutta et al. [27], and Sogut [28] also successfully simulated both behaviors of unstrengthened and strengthened RC beams with this approach. Moreover, overall predicted behavior was in good agreement with the experimental results of Barros and Dalfre [15] (see FE validation section).

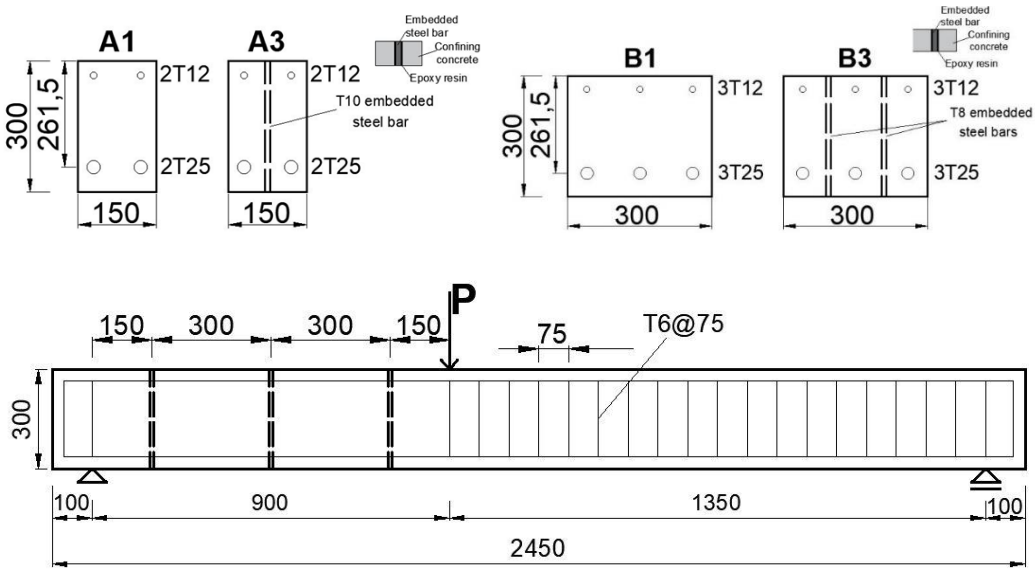

Fig. 1. Cross-sections and elevation of RC beams tested by Barros and Dalfre [15] (dimensions in mm)

Table 1. Material properties of steel bars

Property	6 mm steel bars	8 mm steel bars	10 mm steel bars	12 mm steel bars	25 mm steel bars
Young's modulus (MPa)	206070	212360	205160	206620	216190
Yield strength (MPa)	559.14	566.5	541.6	484.68	507.68
Ultimate strength (MPa)	708.93	675.73	643.23	655.53	743.41

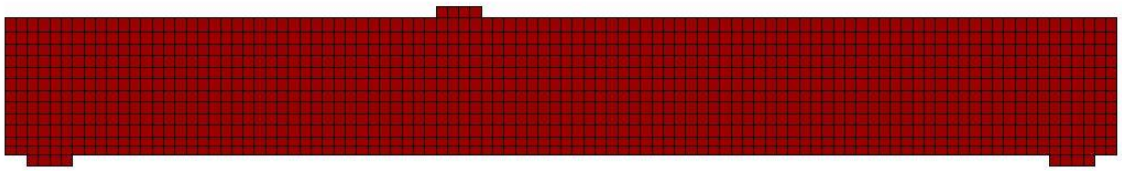

Fig. 2. FE model of the beams tested by Barros and Dalfre [15]

3.2. Material modeling

The stress-strain curve proposed by Thorenfeldt et al. [26] was used to model concrete compression behavior. The curve is defined as follows:

$$f_c = -\left(\frac{\varepsilon_c}{\varepsilon_p}\right) f_p \frac{n}{n - 1 + \left(\frac{\varepsilon_{ci}}{\varepsilon_p}\right)^{nk}} \quad (1)$$

where f_c (MPa) characterizes the concrete compressive stress at a certain strain εc (mm/mm), f_p (MPa) is the concrete cylinder compressive strength and ε_p (mm/mm) is the corresponding strain; n and k are parameters equal to $0.8 + f_p/17$ and $0.67 + f_p/62$, respectively.

The concrete softening in compression was considered by using the model proposed by Vecchio and Collins [30]. It was assumed that concrete's behavior in tension was linear elastic before the development of cracks. A bilinear tension softening model adapted from CEB-FIP Model Code [31] by VecTor2 was used to simulate the behavior of concrete after the development of cracks [22].

The material model used for the steel reinforcement, support, and loading of steel plates consisted of three stages. The stress-strain model had a linear-elastic line until yield stress. This was followed by a plateau and a strain-hardening stage, respectively. The constitutive material and analysis models for the proposed FE model together with the main input parameters are given in Table 2. It should be noted that most of the material and analytical models used to develop the FE model were default models recommended by VecTor2 software [22].

Table 2. FE modeling

Concrete models		**Reinforcement models**			
Concrete pre- and post-Peak	Popovics (HSC) Base Curve	**Hysteretic response**	Bauschinger Effect		
Compression softening	Vecchio 1992-B (e1-e0-Form)	**Dowel action**	Tassios (crack slip)		
Tension stiffening	Modified Bentz 2003	**Buckling**	Modified Dhakal-Maekawa		
Tension softening	Bilinear	**Main input parameters**			
Confined strength	Kupfer/Richart	**f_c (MPa)**	**f_t (MPa)**	**E_c (MPa)**	**Poisson's ratio**
Dilation	Variable-Isotropic	30.78	$0.6\sqrt{f_c}$	$3320\sqrt{f_c + 6900}$	0.15
Cracking criterion	Mohr-Coulomb (Stress)	**Analysis models**			
Crack stress calculation	Basic (DSFM/MCFT)	**Strain history**	The previous loading considered		
Crack width check	Agg. / 2.5	**Cracking spacing**	CEB-FIP 1978-Deformed		
Crack width check	Walraven	**Maximum number of iterations**	100		
Creep and Relaxation	Not considered	**Convergence limit**	1.00001		
Hysteretic response	Nonlinear/w-Plastic offsets	**Structural damping**	Not considered		
Default models (VecTor2)		**Geometric nonlinearity**	Considered		
		Convergence criteria	Displacements-Weighted average		

4. FE results and discussion

4.1. FE model validation

The experimental results of Barros and Dalfre [15] in terms of ultimate shear force capacity and corresponding displacement at ultimate shear force capacity were compared with the corresponding FE model results to confirm the accuracy of the proposed FE model. These values are given in Table 3. As reported in Table 3, the predicted-to-experimental shear force at failure has a mean value of 1.04 with a standard deviation of 0.05. This confirms the accuracy of the FE model in terms of capturing ultimate shear force capacity. The corresponding value for displacement at ultimate shear force capacity is 0.93 with a standard deviation of 0.07.

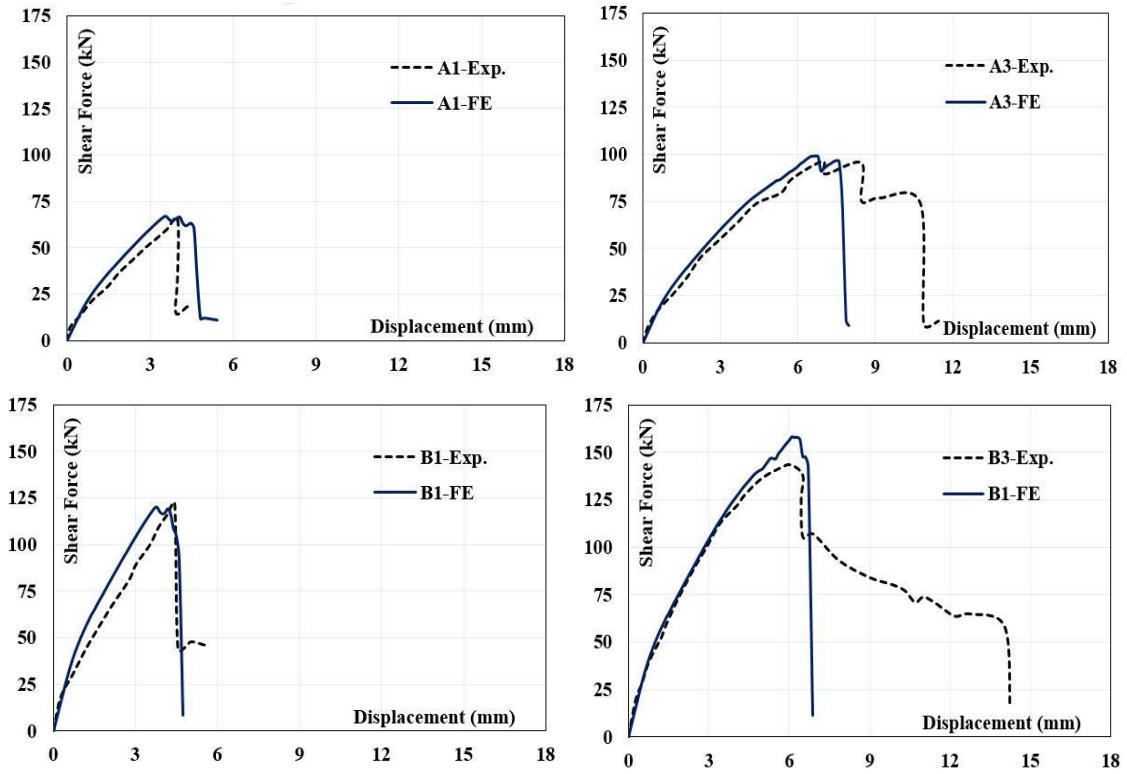

Fig. 3. Experimental [13] and FE-predicted shear force-displacement curves

Table 3. Experimental results of Barros and Dalfre [15] vs. FE results

Beam ID	Shear force at failure (kN)			Displacement at peak shear force (mm)		
	Experimental	FE Prediction	FE/Exp.	Experimental	FE Prediction	FE/Exp.
A1	65.3	67.1	1.03	4.01	3.58	0.89
A3	96.5	99.3	1.03	6.97	6.68	0.96
B1	122.0	120.2	0.99	4.45	3.78	0.85
B3	143.3	157.9	1.10	6.06	6.08	1.00
Mean			1.04			0.93
Standard deviation			0.05			0.07

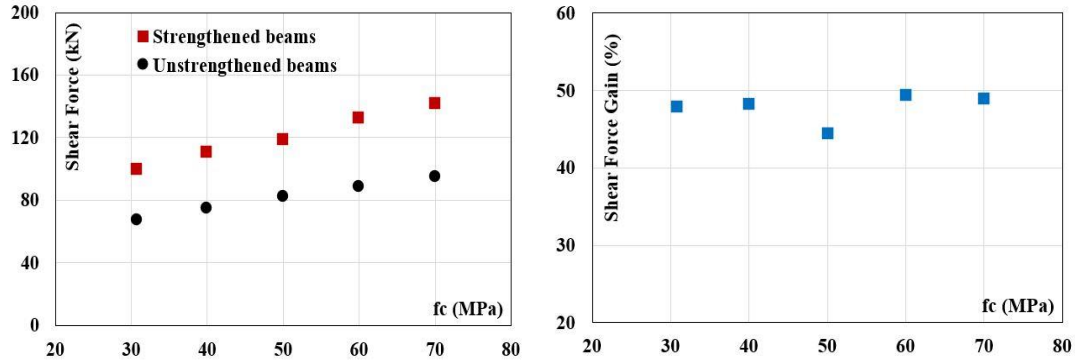

(a) (b)

Fig. 4. Concrete compressive strength vs. (a) shear force capacity and (b) the percentage of shear strength improvement due to embedded steel bars

Fig. 3 compares the experimental shear force-displacement curves with the FE-predicted shear force-displacement curves. As shown in Fig. 3, the overall predicted shear force-displacement response is in good correlation with the experimental shear force-displacement response. The initial (i.e., prior to cracking) stiffness was captured well by the FE model. This can be explained by well-modeled boundary conditions combined with elastic constants. After the development of cracks, a transition in shear force-displacement curves started from a linear to a nonlinear response. It was observed that cracks continued to diminish stiffness until failure took place. Finally, the shear force capacity of the beam was exceeded, and shear failure took place. This was also indicated by a sudden drop in the shear force-displacement curves.

4.2. Effect of concrete compressive strength

To investigate the effect of concrete compressive strength on the strengthened behavior, five different cylinder concrete compressive strength values were studied. These values varied between 30.78 and 70 MPa. The FE-modeled beams for conducting a parametric study on the effect of concrete compressive strength were identical to A1 and A3. The only considered parameter was concrete compressive strength, and hence other parameters were not changed. Figs. 4a and 4b show variations in shear force capacity and percentage of shear strength improvement due to embedded steel bars, respectively, with cylinder concrete compressive strength. Both shear force capacities of unstrengthened and strengthened beams almost linearly increased with a raise in the concrete compression strength from 30.78 to 70 MPa, as shown in Fig. 4a. The shear force capacity of unstrengthened and strengthened beams increased from 67.1 to 94.8 kN (by %41.3) and from 99.3 to 141.3 kN (by %42.3), respectively. Fig. 4b shows that the variation in the percentage of shear strength improvement due to embedded steel bars remained nearly constant as concrete strength increased.

4.3. Effect of beam width

The validated FE model was utilized to further examine the influence of the beam width on the strengthened behavior. The beams modeled to conduct a parametric study on the effect of beam width were also nominally identical to A1 and A3 but had different widths varying between 75 and 525 mm. The variations in shear force capacity and percentage of shear strength improvement due to embedded steel bars, with beam width, are presented in Figs. 5a and 5b, respectively. An increase in beam width from 75 to 525 mm led to an increase in the shear force capacity from 74.5 to 147.9 kN for strengthened beams. The corresponding increase in the shear force capacity for unstrengthened beams was from 43.4 to 134.1 kN. As can be seen in Fig. 5b, an increase in beam width from 75 to 525 mm instigates a reduction in the percentage of shear strength improvement due to embedded steel bars. The shear strength improvement decreased from 71.5 to

10.3% when the beam width was increased from 75 to 525 mm. This can be explained by the fact that an increase in the beam width resulted in an increased concrete contribution to the shear resistance of the beam.

4.4. Size effect

To investigate the size effect in RC beams strengthened in shear with embedded steel bars, nominally identical beams to A1 and A3 were modeled in VecTor2 software. All dimensions of A1 and A3 together with support and loading steel plates were scaled by a scale factor that varied between 0.5 and 2. For example, the overall depth of the modeled beams varied from 150 to 600 mm. The cross-sectional area of longitudinal tension and compression reinforcement, steel shear links, and embedded steel bars were also scaled by the above scale factors. Thus, the reinforcement ratios were kept constant. As shown in Fig. 6a, shear stress at failure decreased by 42% and 38.5% for unstrengthened and strengthened beams, respectively, with increasing effective depth from 131 to 523 mm. The decrease in the shear stress at failure can be explained by the size effect [33, 34]. It should be noted that the above results are consistent with the results of former studies on unstrengthened and FRP-strengthened beams [12, 18, 33, 34, 35].

Fig. 6b demonstrates a variation in percentage shear strength improvement due to embedded steel bars with effective beam depth. Shear strength improvement due to embedded steel bars increased from 20.3% to 27.6% with an increase in the effective depth from 131 to 261.5 mm. However, the corresponding shear strength improvement decreased from 47.9% to 27.6% with increasing effective depth from 261.5 mm to 523 mm. These results are similar to those of Qapo et al. [35]. It was reported that EB FRP-strengthened pre-stress concrete (PC) beams without steel shear links had the same trend as in Fig. 6b. The initial increase was explained by the fact that the size effect tended to be insignificant, and thus, an increase in the bond length instigated an improvement in shear force [35]. The latter decrease was attributed to the size effect [35]. This might be explained by the fact that an increase in the beam size resulted in an increase in concrete contribution to the shear resistance of the beam. Table 4 presents the shear components of the beams. The contribution of embedded steel bars to shear resistance (V_e) was calculated by subtracting concrete contribution (V_c), which is equal to unstrengthened shear force capacity, from strengthened shear force capacity. As can be seen in Table 4, the percentage of concrete contribution to shear resistance increased from 67.6 to 78.4% with increasing beam size. Nevertheless, size effect in DE-strengthened beams without existing steel shear links need to be experimentally investigated.

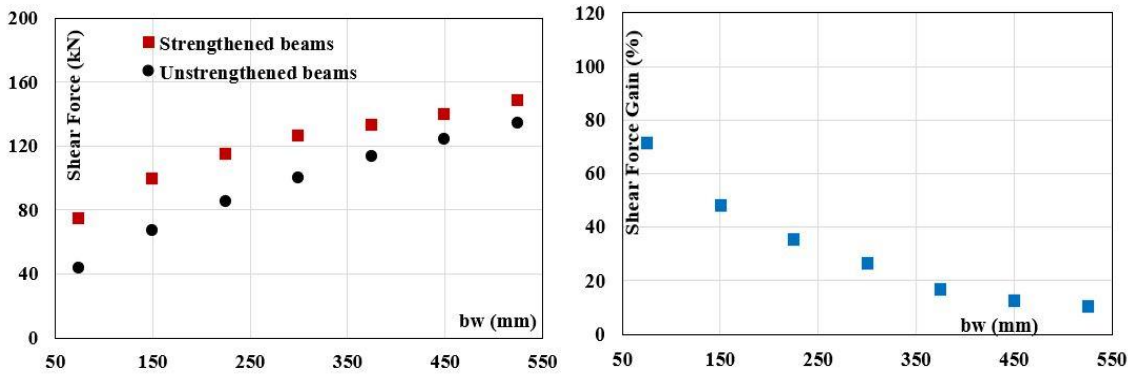

(a) (b)

Fig. 5. Effect of beam width on (a) shear force capacity and (b) percentage of shear strength improvement due to embedded steel bars

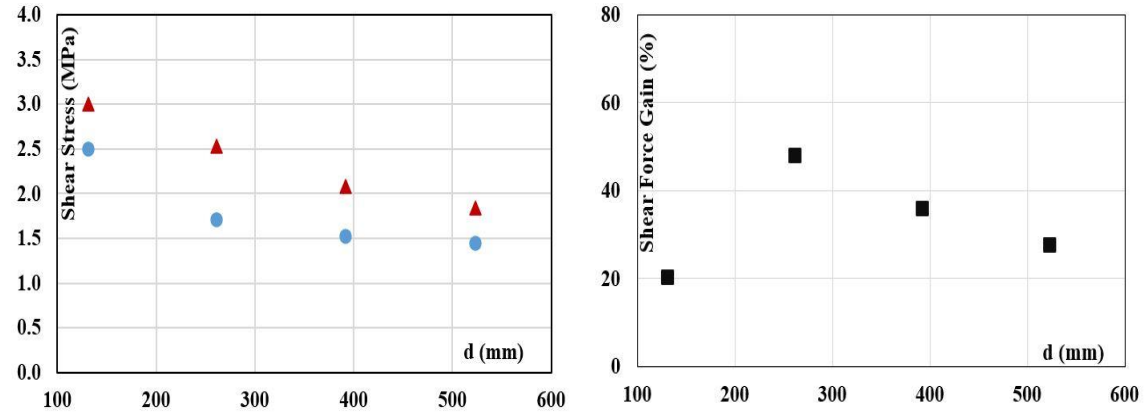

(a) (b)

Fig. 6. Effective depth vs. (a) shear force capacity and (b) the percentage of shear strength improvement due to embedded steel bars

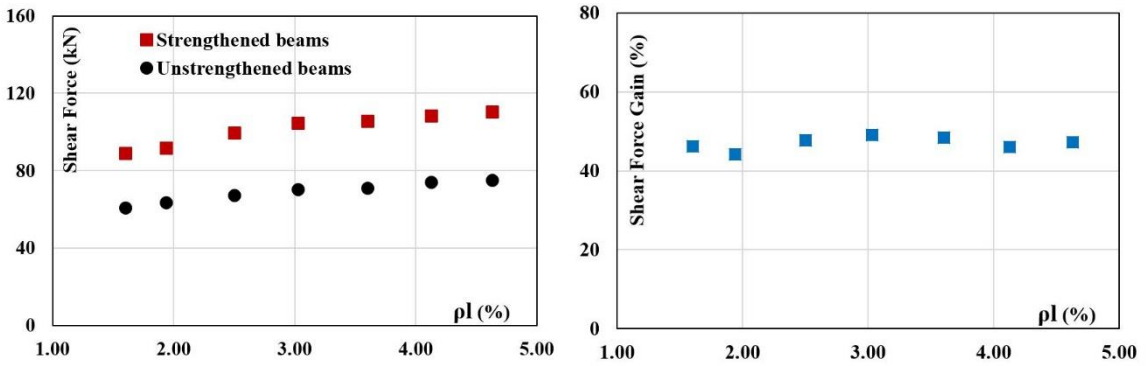

(a) (b)

Fig. 7. Tension reinforcement ratio vs. (a) shear force capacity and (b) percentage of shear strength improvement due to embedded steel bars

Table 4. Shear components of beams

Beam ID	V_{total} (kN)	V_c (kN)	V_e (kN)	V_c (%)	V_e (%)
A1-1.0	67.1	67.1	-	100	0
A3-1.0	99.3	67.1	32.2	67.6	32.4
A1-1.5	134.8	134.8	-	100	0
A3-1.5	183.2	134.8	48.4	73.6	26.4
A1-2.0	226.8	226.8	-	100	0
A3-2.0	289.3	226.8	62.5	78.4	21.6

4.5. Effect of tension reinforcement ratio

The effect of the tension reinforcement ratio on the strengthened behavior was examined by considering different tension reinforcement ratios in a range between 1.60% and 4.63%. The modeled beams were also nominally identical to A1 and A3. Fig. 6a shows the variations in the shear force capacity of unstrengthened and strengthened beams with a tension reinforcement ratio. As can be seen in Fig. 7a, an increase in tension reinforcement ratio from 1.6% to 4.63% resulted in an improvement in shear force capacity from 60.8 kN to

74.9 kN and from 89 kN to 110.3 kN for unstrengthened and strengthened beams, respectively. Fig. 7b demonstrates the relationship between the percentage of shear strength improvement and the tension reinforcement ratio. The percentage of shear strength improvement was almost constant with an increasing tension reinforcement ratio. For example, the corresponding values were 46.4% and 47.4% for the beams with a tension reinforcement ratio of 1.6% and 4.63%, respectively. This result is crucial since it has been demonstrated that tension reinforcement did not have a significant impact on shear force improvement due to embedded steel bars. The effect of tension reinforcement can only change the failure mode of the strengthened beams. Furthermore, this result is consistent with the results of Sogut et al. [4] reported for DE FRP-strengthened beams with existing steel shear links. It was demonstrated that the tension reinforcement ratio did not play a vital role in increasing the shear strength of DE FRP-strengthened beams.

5. Conclusions

This paper presents a two-dimensional FE model that was developed for DE steel strengthened-RC rectangular beams without steel shear links and validated against published experimental results. Furthermore, the validated FE model was used to shed light on the impacts of concrete compressive strength, beam width, beam size, and tension reinforcement ratio on the strengthened behavior. As previously mentioned, the DE technique offers a great solution for shear-deficient RC beams where EB and NSM techniques cannot be applied. It is believed that the investigated parameters in this study can be considered in terms of the development of a design model for DE-strengthened RC beams without existing steel shear links. Moreover, the developed FE model in this study can provide accurate predictions for the behavior of DE-strengthened RC beams.

The following findings are obtained from this study:

1. The predicted-to-experimental shear force at failure has a mean value of 1.04 with a standard deviation of 0.05. This confirms the accuracy of the FE model in terms of capturing ultimate shear force capacity. The corresponding value for displacement at ultimate shear force capacity is 0.93 with a standard deviation of 0.07.
2. The predicted shear force capacity of unstrengthened and strengthened beams increased by %41.3 and %42.3, respectively, when the concrete compressive strength was increased from 30.78 to 70 MPa. The percentage of shear strength improvement due to embedded steel bars was almost constant with an increase in the concrete strength.
3. An increase in beam width from 75 to 525 mm led to an increase in the shear force capacity from 74.5 to 147.9 kN for strengthened beams. The corresponding increase in the shear force capacity for unstrengthened beams was from 43.4 to 134.1 kN. The shear strength improvement decreased from 71.5 to 10.3% when the beam width was increased from 75 to 525 mm.
4. Shear stress at failure decreased by 42% and 38.5% for unstrengthened and strengthened beams, respectively, with a raise in effective depth from 131 to 523 mm. However, the corresponding shear strength improvement decreased from 47.9% to 27.6% as effective depth was raised from 261.5 mm to 523 mm.
5. Shear force capacities of both unstrengthened and strengthened beams increased when the tension reinforcement ratio was increased. However, an increase or decrease in the tension reinforcement ratio did not play a significant role in gaining shear strength due to embedded steel bars. This demonstrated that the tension reinforcement ratio only effects the failure mode of the DE-strengthened beam.

Declaration of conflicting interests

The author(s) declared no potential conflicts of interest with respect to the research, authorship, and/or publication of this article.

References

[1] Dirar S, Lees JM, Morley CT (2013) Pre-cracked RC T-beams repaired in shear with prestressed CFRP straps. ACI Structural Journal 110(5):855-866.

[2] Dirar S, Lees JM, Morley CT (2012) Pre-cracked RC T-beams repaired in shear with externally bonded CFRP sheets. ACI Structural Journal 109(2):215-223.

[3] Valerio P, Ibell TJ, Darby A (2009) Deep embedment of FRP for concrete shear strengthening. Structures and Buildings 162(5):311-321.

[4] Sogut K, Dirar S, Theofanous M, Faramarzi, A. Nayak AN (2021) Effect of transverse and longitudinal reinforcement ratios on the behavior of RC T-beams shear strengthened with embedded FRP bars. Composite Structures 262:113622.

[5] Mofidi A, Chaallal O, Benmokrane B, Neale K (2012) Experimental tests and design model for RC beams strengthened in shear using the embedded through-section FRP method. ASCE Journal of Composites for Construction 16(5):540-550.

[6] Valerio P, Ibell T (2003) Shear strengthening of existing concrete bridges. Structures and Buildings 156(1):75-84.

[7] Chaallal O, Mofidi A, Benmokrane B, Neale K (2011) Embedded through-section FRP rod method for shear strengthening of RC beams: performance and comparison with existing techniques. ASCE Journal of Composites for Construction 15(3):374-383.

[8] Breveglieri M, Aprile A, Barros JAO (2015) Embedded through-section shear strengthening technique using steel and CFRP bars in RC beams of different percentages of existing stirrups. Composite Structures 126:101-113.

[9] Jemaa Y, Jones C. Dirar S (2015) Deep embedment strengthening of full-scale shear deficient reinforced concrete beams. In: Proceedings of the 12th International Symposium on Fiber Reinforced Polymers for Reinforced Concrete Structures (FRPRCS-12), Nanjing, China, pp. 1-6.

[10] Dirar S, Theofanous M (2017) Large-scale reinforced concrete T-beams strengthened in shear with embedded GFRP bars. In: Proceedings of the 8th International Conference on Advanced Composites in Construction (ACIC 2017), Sheffield, UK, pp. 114-119.

[11] Raicic V, Ibell T, Darby A, Evernden M, Orr J (2017) Effectiveness of the deep embedment (DE) technique for shear strengthening of reinforced concrete continuous beams. In: Proceedings of the 8th International Conference on Advanced Composites in Construction (ACIC 2017), Sheffield, UK, pp. 6.

[12] Qapo M, Dirar S, Jemaa Y (2016) Finite element parametric study of reinforced concrete beams shear strengthened with embedded FRP bars. Composite Structures 149:93-105.

[13] Sogut K, Dirar S, Theofanous M, Faramarzi A (2019) Effect of existing steel-to-embedded FRP shear reinforcement ratio on the behavior of reinforced concrete T-beams. In: Proceedings of the 9th International Symposium on Advanced Composites in Construction (ACIC 2019), Birmingham, UK, pp. 11-16.

[14] Bui LVH, Stitmannaithum B, Ueda T (2020) Experimental investigation of concrete beams strengthened with embedded through-section steel and FRP bars. ASCE Journal of Composites for Construction 24(5):04020052.

[15] Barros JAO, Dalfré GM (2013) Assessment of the effectiveness of the embedded through-section technique for the shear strengthening of reinforced concrete beams. Strain 49(1):75–93.

[16] Bhanugoban M, Yapa HD, Dirar S (2021) Efficient shear retrofitting of reinforced concrete beams using prestressed deep embedded bars. Engineering Structures 246:113053.

[17] Qin S, Dirar S, Yang J, Chan AHC, Elshafie M (2015) CFRP shear strengthening of reinforced-concrete T-beams with corroded shear links. ASCE Journal of Composites for Construction 19(5):04014081.

[18] Sogut K, Dirar S, Theofanous M, Faramarzi A (2019) Size effect in shear-deficient reinforced concrete T-beams strengthened with embedded FRP bars. In: Proceedings of the 14th International Symposium on Fiber-Reinforced Polymer Reinforcement for Concrete Structures, (FRPRCS-14), Belfast, UK.

[19] Caro M, Dirar S, Quinn A, Yapa H (2021) Shear strengthening of existing reinforced concrete beams with embedded bars – an overview. In: Proceedings of the Institution of Civil Engineers – Structures and Buildings, pp. 1-14, DOI: 10.1680/jstbu.20.00169.

[20] Vecchio FJ (2020) Disturbed stress field model for reinforced concrete: formulation. ASCE Journal of Structural Engineering 126(9):1070-1077.

[21] Vecchio FJ, Collins MP (2986) The modified compression field theory for reinforced concrete elements subject to shear. ACI Journal 83(2):219-231.

[22] Wong PS, Vecchio FJ, Trommels H (2013) VecTor2 & FormWorks User's Manual (2nd edition). The University of Toronto.

[23] Bažant ZP, Oh BH (1983) Crack band theory for fracture of concrete. Matériaux et Constructions 16(3):155-177.

[24] Dirar S, Lees JM, Morley CT (2013) Phased nonlinear finite-element analysis of pre-cracked RC T-beams repaired in shear with CFRP sheets. ASCE Journal of Composites for Construction 17(4):476-487.

[25] Sogut, K., Dirar, S., Theofanous, M., Faramarzi, A. (2022). Effect of FRP bar type on the behaviour of shear-strengthened reinforced concrete T-beams. In: Ilki, A., Ispir, M., Inci, P. (eds) 10th International Conference on FRP Composites in Civil Engineering. CICE 2021. Lecture Notes in Civil Engineering, vol 198. Springer, Cham. https://doi.org/10.1007/978-3-030-88166-5_117

[26] Godat A, Chaallal O, Neale KW (2013) Nonlinear finite element models for the embedded through-section FRP shear-strengthening method. Computers & Structures 119:12-22.

[27] Dutta B, Sogut K, Dirar S, Nayak AN, Nanda B, Theofanous M, Faramarzi A (2019) Nonlinear finite element analysis of reinforced concrete beams strengthened in shear with embedded steel bars. The 9th International Conference on Advanced Composites in Construction (ACIC 2019), Birmingham, UK.

[28] Sogut K (2022) Effect of tension reinforcement ratio on the behavior of DE-strengthened-RC beams without steel shear reinforcement. In: Proceedings of 4th International October 29 Scientific Research Symposium, Adana, Turkey.

[29] Thorenfeldt E, Tomaszewicz A, Jensen JJ (1987) Mechanical properties of high-strength concrete and applications in design. In: Proceedings of the Symposium on Utilization of High Strength Concrete, Stavanger, pp. 149–159.

[30] Vecchio FJ, Collins MP (1993) Compression response of cracked reinforced concrete. ASCE Journal of Structural Engineering 119(12):3590-3610.

[31] CEB-FIP Model Code 1990. Thomas Telford Services Ltd., London.

[32] Bentz EC (2005) Explaining the riddle of tension stiffening models for shear panel experiments. ASCE Journal of Structural Engineering 131(9):1422–1425.

[33] Kani GNJ (1967) How safe are our large reinforced concrete beams? ACI Journal Proceedings 64(3):128-141.

[34] Bažant ZP, Kim JK (1984) Size effect in shear failure of longitudinally reinforced beams. ACI Journal Proceedings 81(5):456-468.

[35] Qapo M, Dirar S, Yang J, Elshafie MZEB (2015) Nonlinear finite element modelling and parametric study of CFRP shear-strengthened prestressed concrete girders. Construction and Building Materials 76:245-255.